Effects of non-pairwise repulsion on nanoparticle assembly

Sawyer S. Hopkins, Amitabha Chakrabarti, and Jeremy D. Schmit

View Online   Export Citation   CrossMark

The Journal
of Chemical Physics

Submit Today

The Emerging Investigators Special Collection and Awards
Recognizing the excellent work of early career researchers!

AIP Publishing

Effects of non-pairwise repulsion on nanoparticle assembly

View Online Export Citation CrossMark

Sawyer S. Hopkins, Amitabha Chakrabarti, and Jeremy D. Schmit[a] (ID)

AFFILIATIONS

Department of Physics, Kansas State University, Manhattan, Kansas 66506, USA

[a]schmit@phys.ksu.edu

ABSTRACT

Electrostatic interactions provide a convenient way to modulate interactions between nanoparticles, colloids, and biomolecules because they can be adjusted by the solution pH or salt concentration. While the presence of salt provides an easy method to control the net interparticle interaction, the nonlinearities arising from electrostatic screening make it difficult to quantify the strength of the interaction. In particular, when charged particles assemble into clusters or aggregates, nonlinear effects render the interactions strongly non-pairwise. Here, we report Brownian dynamics simulations to investigate the effect that the non-pairwise nature of electrostatic interactions has on nanoparticle assembly. We compare these simulations to a system in which the electrostatics are modeled by a strictly pairwise Yukawa potential. We find that both systems show a narrow range in parameter space where the particles form well-ordered crystals. Bordering this range are regions where the net interactions are too weak to stabilize aggregated structures or strong enough that the system becomes kinetically trapped in a gel. The non-pairwise potential differs from the pairwise system in the appearance of an amorphous state for strongly charged particles. This state appears because the many-body electrostatic interactions limit the maximum density achievable in an assembly.

Published under license by AIP Publishing. https://doi.org/10.1063/1.5092130

I. INTRODUCTION

The self-assembly of particles into ordered structures requires a tuning of the net interparticle potential such that the interactions are sufficiently strong to stabilize the structure, yet thermally reversible so that defects can be removed.[1–3] Electrostatic interactions are a convenient mechanism for this tuning since they can be adjusted by modifying the surface chemistry, solution pH, or salt concentration.[4] Electrostatic tuning played a central role in early descriptions of colloid stability where electrostatic repulsion was used as a balance against fixed attractive interactions.[5,6] The DLVO (Derjaguin, Landau, Verwey, and Overbeek) framework has remained an important guide for the solubility of charged particles; however, important differences emerge when considering particles on the nanometer scale such as biomolecules or nanoparticles. For starters, the long-ranged van der Waals attraction becomes less important than short-ranged interactions such as H-bonds and the hydrophobic effect. This has inspired numerous studies of the competition between short-range attraction and long-range repulsion, where the repulsion is modeled using a repulsive Yukawa potential.[7–13] This qualitatively captures the effects of Coulomb repulsion screened by salt because the Yukawa potential emerges from the small potential limit of the Poisson-Boltzmann (PB) equation. However, as the density of charges increases, such as when the particles aggregate, the electrostatic potential rises above the acceptable range for the small potential (Debye-Huckel) treatment. While this has the expected effect of causing quantitative discrepancies as the nonlinearities of the PB equation take effect, a less intuitive consequence is that aggregation qualitatively changes the nature of the interparticle interaction. This is because aggregation compresses the screening layer around each particle resulting in a *favorable* Coulomb interaction, but incurring a large entropic penalty.[14]

An important consequence of the transition to entropy-dominated electrostatics is that electrostatic repulsion can no longer be treated in a pairwise fashion (i.e., screened Coulomb interactions). Instead, the electrostatic interactions are delocalized through the screening layers. From a theoretical viewpoint, this has mixed effects. On one hand, delocalization of the interaction means that the electrostatic free energy is insensitive to the precise location of charges, which makes the calculation amenable to mean-field treatments.[15,16] On the other hand, it means that the calculation must account for the non-pairwise nature of the interactions.

The purpose of this paper is to explore how non-pairwise repulsion contributes to nanoparticle assembly and aggregation. From a thermodynamic point of view, we expect that non-pairwise repulsion will destabilize densely packed structures since each additional interparticle contact reduces the affinity of all previous contacts. Usually, when an aggregation process terminates with the formation of a gel or amorphous aggregate, it is assumed that this state is a kinetic trap and the thermodynamic ground state is an ordered crystal that maximizes the favorable contact energy. In the presence of non-pairwise repulsive interactions, this is not necessarily the case because the nonlinear repulsion can destabilize the higher density structure. Note that a similar effect can also emerge from pairwise interactions if the range of the repulsion is long enough to permit next-nearest-neighbor interactions. However, non-pairwise additivity means that there can be a limit on the packing density even if the screening length is smaller than the particle size.

Non-pairwise interactions are also expected to have a significant effect on the kinetics of assembly because particles attempting to bind to a cluster will be less likely to explore higher density states. This will provide a bias against ordered crystals even if these states are the thermodynamic minimum. The bias against dense states will be particularly significant in the nucleation phase, especially if the critical nucleus is small enough that bulk-like interactions have not yet emerged (as is the case in protein crystals[17]).

In a previous paper, we explored the effect of electrostatic interactions on the competition between crystallization and gelation.[14] That work used the simplified criteria that a gel would emerge when a single interparticle contact provides enough binding energy to pay the translational entropy cost of removing a monomer from solution. In that model, the window of successful crystallization conditions is bounded by the stability of the crystal and the instability of the solution with respect to two-body interactions. This window expands when the particle charge and salt concentration are simultaneously increased such that the net interaction strength is maintained but the repulsive interactions are more nearly pairwise.[14] Here, we report Brownian dynamics simulations that qualitatively confirm these predictions with a crystallization window that grows narrower as the non-pairwise character of the interactions increases. However, our simulations also show the emergence of an amorphous structure that is not present when the interactions are strictly pairwise, indicating that non-pairwise interactions have destabilized the high density states required for crystallization.

II. METHODS

A. Brownian dynamics simulations model a system with a hard core, short range attraction, and electrostatic repulsion

Our simulations consist of a system of particles evolving according to the Langevin equation[18]

$$m_i \ddot{r}_i = F_i(r) - \Gamma \dot{r}_i + \xi_i(t), \qquad (1)$$

where F_i is the systematic force, ξ_i is the stochastic force, m_i is the particle mass, and Γ is the friction coefficient. The systematic

force can be subdivided into electrostatic and nonelectrostatic contributions. The non-electrostatic forces consist of a short ranged attractive interaction with a hard core repulsion, $F_a(r)$, while the electrostatic part, $F_{es}(r)$, is repulsive at all distances. The short range attractive force encompasses H-bond, van der Waals, and hydrophobic effects and was modeled using an extended Lennard-Jones (LJ) potential of the form shown in Eq. (2), in which the particle diameter $\sigma = 1$, $k_B T = 1$, and ϵ is used as a control variable to tune the attractive strength of the force,

$$V_a(r) = -\int F_a(r)\mathrm{d}r = 4\epsilon k_B T \left[\left(\frac{\sigma}{r}\right)^{50} - \left(\frac{\sigma}{r}\right)^{25} \right]. \qquad (2)$$

The 25/50 powers were selected to avoid anomalies that have been reported in hard-core behavior with smaller exponents.[19–21]

The simulations consisted of 2500 uniform spherical particles in a cubic box at a volume concentration of 9.5%. Other concentrations were not attempted as the primary effect would be to alter the volume fractions occupied by the dense and dilute states with minimal effect on the phase boundaries. The particles evolved through the integration of Eq. (1) with a time step of 0.001 (unitless). Periodic boundary conditions were implemented across all surfaces. Integration was halted for all trials after 10^8 integration cycles. The attractive potential strength, ϵ, was varied in $0.25 K_B T$ increments. To assist in the initial nucleation of crystalline structures, a $4 \times 4 \times 4$ primitive cubic seed crystal was placed in the center of the box at the beginning of each simulation.

B. Electrostatic repulsion is computed from the volume accessible to the screening layer

Here, we derive an effective potential intended to qualitatively capture the effects of screening layer distortion on the electrostatic free energy. The full electrostatic free energy is the sum of the Coulomb energy and the entropy of the salt, $F_{ES} = E_{\text{Coul}} - TS_{\text{salt}}$. These terms are given by[22–24]

$$E_{Coul} = \frac{1}{2\epsilon} \int_V |\nabla \Psi(r)|^2 \mathrm{d}V, \qquad (3)$$

$$-TS_{\text{salt}} = k_B T \int_V \left[c_+ ln\left(\frac{c_+}{c_s}\right) - c_+ + c_s \right] + \left[c_- ln\left(\frac{c_-}{c_s}\right) - c_- + c_s \right] \mathrm{d}^3 r, \qquad (4)$$

where Ψ is the electrostatic potential, $c_\pm$ are the local concentrations of cations and anions, ϵ is the local permittivity, and c_s is the salt concentration in a reservoir far from any charges. For monovalent salt, minimization of F_{ES} with respect to the ion concentrations yields

$$c_\pm = c_s e^{\mp e\Psi/k_B T}. \qquad (5)$$

These concentrations can be plugged into the Poisson equation to yield the well-known PB equation for the electrostatic potential. Rather than taking the computationally demanding step of solving the PB equation at each time step in the simulation, we employ a series of approximations that allow for a closed form free energy expression while retaining the essential nonlinearities.

The first approximation is to neglect the Coulomb energy term, which is a minor contribution to the free energy in the aggregated states that are of primary interest here.[14,15] The neglect of the Coulomb energy will have the effect of artificially narrowing

the crystallization window since this term is attractive for dense structures and repulsive for more diffuse ones.[14]

The next approximation is to model the screening layer with a step function profile. That is, we approximate the potential to have a constant value $\bar{\Psi}$ within a distance a of the particle surface and $\Psi = 0$ outside this distance.[25] The potential within the screening layer can be determined from the condition that the layer contains enough charge to neutralize the particle[25]

$$Q = -v(c_+ - c_-) = 2vc_s \sinh\left(\frac{e\bar{\Psi}}{k_B T}\right), \qquad (6)$$

where v is the volume accessible to the ions in the screening layer. With the constant potential approximation, the integrals in Eq. (4) are easily evaluated and we find that the electrostatic free energy is

$$\frac{F_{ES}}{k_B T} \simeq -S_{\text{salt}}/k_B = Q\left(\sinh^{-1}\left(\frac{1}{\zeta}\right) - \sqrt{1 + \zeta^2} + \zeta\right), \qquad (7)$$

where $\zeta = 2vc_s/Q$. The electrostatic free energy associated with a particular macroion depends on the volume v accessible to that ion's screening layer. This volume, in turn, will depend on the location of neighboring particles, which can occupy volume that would be otherwise accessible.

The restriction of the screening layer volume is shown schematically in Fig. 1. For the illustrated two-body interaction, the volume accessible to each screening layer is

$$v = v_t - v_p - \frac{1}{2}v_e, \qquad (8)$$

where v_t is the total volume inside a sphere of radius $R + a$, $v_p = 4\pi R^3/3$ is the volume of the macroion, v_e is the volume of the overlapped region, R is the particle radius, and a is the screening layer thickness (see Fig. 1). To simplify the calculation of the screening layer volumes, we conduct our simulations at a salt concentration where the screening layer thickness is ~10% of the particle radius, since for $a/R < 0.15$ it is impossible for the layers of three different macroions to overlap in the same region of space. This allows the overlapped volume to be calculated using pairwise interactions. For a protein i with n neighbors with centers within a sphere of radius $2(R + a)$ from the center of i, the excluded volume can
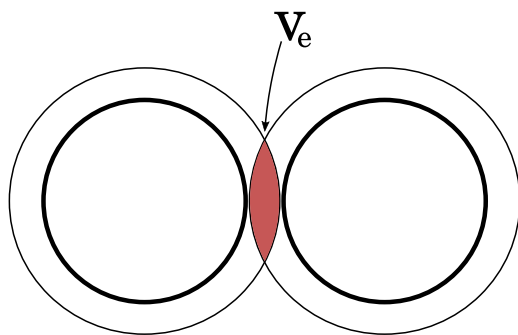
be calculated using the same method as the Asakura-Oosawa-Vrij depletion potential,[26]

$$v_{e_i} = \sum_{j=1}^{n} \frac{4\pi}{3}(R + a)^3\left[1 - \frac{3r_{ij}}{4(R + a)} + \frac{1}{16}\left(\frac{r_{ij}}{(R + a)}\right)^3\right]. \qquad (9)$$

Note that even though the overlapped volume is calculated based on pairwise contacts, the free energy is still non-pairwise due to the nonlinearity of Eq. (7).

In Fig. 2, the approximate expression for the non-pairwise potential is compared to the electrostatic free energy for a linear assembly of nanoparticles and crystals with cubic and hexagonal packing densities. These free energies were obtained by solving the nonlinear Poisson-Boltzmann equation for either a cylindrical geometry or spherical Wigner cells, as described in Ref. 14. In all cases, the approximate potential is less repulsive than the Poisson-Boltzmann free energy, which we attribute to the smoothing effect of the step function approximation. This quantitative discrepancy amounts to a renormalization of the particle charge and does not change the qualitative behavior of the nonadditive potential that is our focus here. A more accurate treatment of the electrostatic free energy would shift the phase boundaries to lower values of the particle charge.

To see the effects of the non-pairwise potential, we run an equivalent set of simulations where the repulsion is described by a strictly pairwise Debye-Huckel potential,

$$U_{dh}(r) = \gamma(Q, c_s)a\frac{e^{-r/a}}{r}. \qquad (10)$$

Here, γ is a renormalized charge that ensures that the pairwise and non-pairwise potentials yield equivalent interaction energies for two isolated particles in contact. This is necessary because the approximations leading to the derivations of both Eq. (7) and the Debye-Huckel potential lead to nonequivalent interactions at the
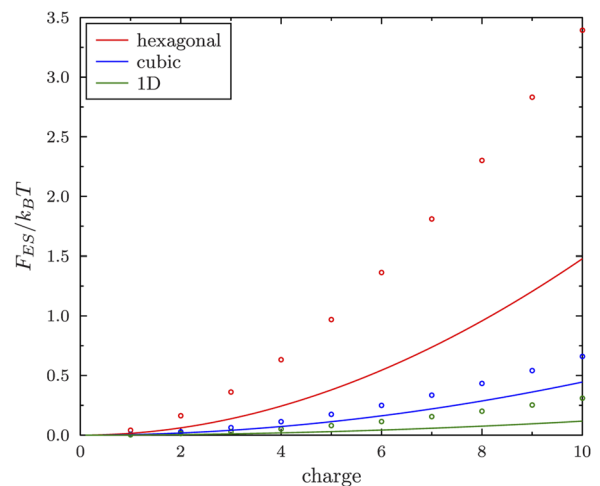

FIG. 1. The excluded volume v_e created via the overlap of electrostatic screening layers.

FIG. 2. Comparison of the approximate electrostatic free energy described by Eq. (7) (lines) to the Poisson-Boltzmann free energy (points) of a line of particles and crystals with cubic and hexagonal packing densities at 1M monovalent salt.

same change and salt concentrations. The renormalized charge is given by

$$\gamma = k_B T \frac{R}{a} e^{R/a} F_{ES}(v_2, Q, c_s), \quad (11)$$

where $F_{ES}(v_2, Q, c_s)$ is evaluated from Eq. (7) using the two-body screening layer volume for two particles in contact ($r = 2R$). In this case, the overlap volume reduces to

$$v_2 = \pi a^2 \left[\frac{4a}{3} + 2R \right]. \quad (12)$$

C. Distinct phases are identified using order parameters sensitive to density and local structure

We characterize the aggregated structure using two order parameters. The first of these is the coordination number, which we calculate by counting the number of particles with a center-to-center distance less than $2(R + a)$ from the reference particle.

While the coordination number provides useful information about the density, we require another metric to probe the structure of an aggregate. One method to do this is to project the nearest-neighbor vectors onto spherical harmonics,[27,28]

$$q_{lm}(i) = \frac{1}{n(i)} \sum_{j=1}^{n(i)} Y_{lm}(r_{ij}). \quad (13)$$

Here, the sum is over the $n(i)$ particles within a center-to-center distance $2(R + a)$ from a particle i. A rotationally invariant version can be constructed as follows:[27]

$$q_l(i) = \sqrt{\frac{4\pi}{2l+1} \sum_{m=-l}^{l} |q_{lm}(i)|^2}. \quad (14)$$

The ability of this metric to resolve distinct phases improves by averaging over the first coordination shell[28]

$$\bar{q}_{lm}(i) = \frac{1}{n(i)} \sum_{k=0}^{n(i)} q_{lm}(k), \quad (15)$$

which can also be cast in a rotationally invariant form

$$\bar{q}_l(i) = \sqrt{\frac{4\pi}{2l+1} \sum_{m=-l}^{l} |\bar{q}_{lm}(i)|^2}. \quad (16)$$

Of the parameters defined by Eq. (16), $\bar{q}_4$ and $\bar{q}_6$ are particularly useful for their ability to resolve common crystal structures such as bcc, fcp, and hcp.[28]

III. RESULTS AND DISCUSSION

A. Particles interacting by pairwise potentials form liquid, crystal, and gel phases

An initial analysis of the simulations was conducted by examining the distribution of nearest neighbor coordination numbers at the end of the simulation. Representative histograms are shown in Fig. 3. For the simulations interacting via a pairwise potential, we identified three distinct states from these distributions.

The liquid phase was defined by coordination histograms where the peak was three or less. This was observed in simulations where the particles are strongly charged and/or have a weak LJ binding energy. Under these conditions, the net interparticle attraction is not sufficient to pay the entropic cost of confining the particles within an aggregated structure, and the contacts we observe are transient collisions. Within the liquid regime, the crystal seeds placed at the start of
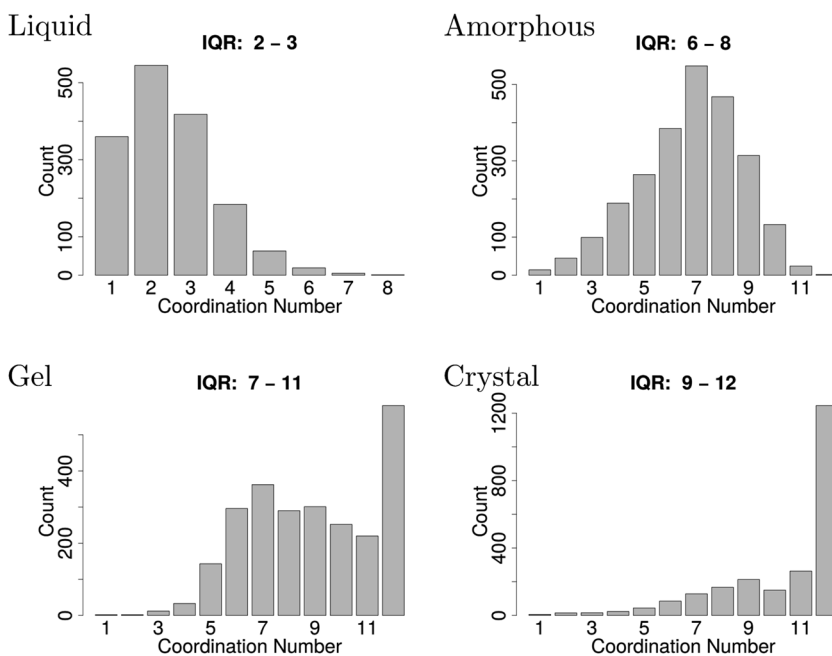

FIG. 3. Representative coordination number distributions for the four states identified in the simulations. The liquid phase is characterized by transient contacts so most particles have only 1–3 nearest neighbors. The amorphous state shows a broad range of coordination numbers, but a conspicuous lack of particles with 11 or 12 nearest neighbors. The gel state also has a broad distribution of coordination numbers along with a second peak at 12 nearest neighbors. This is consistent with hcp and/or fcc packing with a large surface area. However, the inner quartile range (IQR) of particles does not include 12. The crystal phase is dominated by 12-fold coordinated particles, indicating a highly ordered structure and a low surface area.
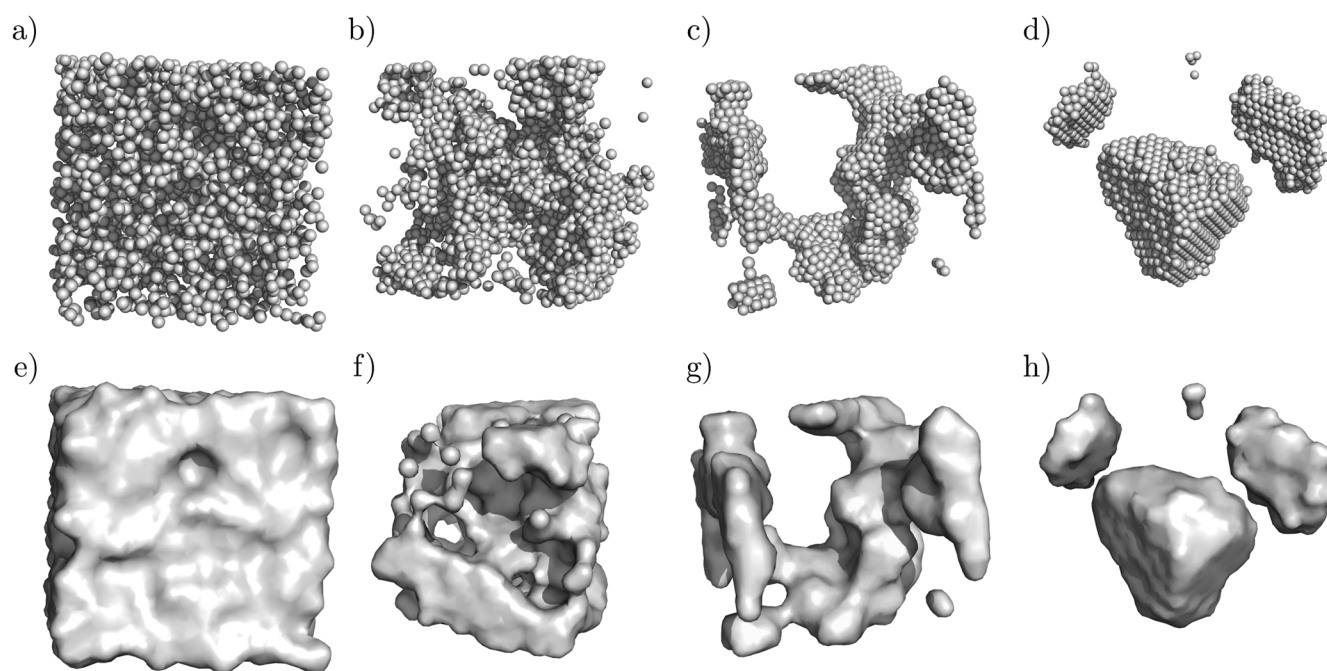
FIG. 4. The structure of the four characterized states shown in both a per particle view [(a)–(d)] and a surface overlay [(e)–(h)]: solution [(a) and (e)], amorphous [(b) and (f)], gel [(c) and (g)], and crystal [(d) and (h)]. Periodic boundary conditions apply to all images.

the simulation dissolve and do not reform (data not shown). However, we cannot rule out the possibility that a larger seed, or one with hexagonal packing, would lead to successful nucleation. In this case, the crystal and/or amorphous phase boundaries would shift leftward at the expense of the solution state.

The crystal phase is distinguishable by the sharp peak in the coordination number histogram at 12. We classify the system in this phase when the inner quartile range (IQR) of coordination numbers contains this peak. The crystal phase is observed when the LJ attraction and electrostatic repulsion combine to give intermediate values

for the net interparticle attraction. These values are strong enough that six bonds are sufficient to surmount the entropic penalty for capturing a particle, yet weak enough that the nucleation of new aggregates is slow on the simulation time scale. This means that the growth is localized to a small number of dominant clusters (see Fig. 4).

The gel state also shows a peak in the coordination number distribution at 12 but differs from the crystal phase in the greater weight of the distribution at smaller numbers. We classify the system in the gel state when the IQR does not contain 12. Visual inspection (Fig. 4)
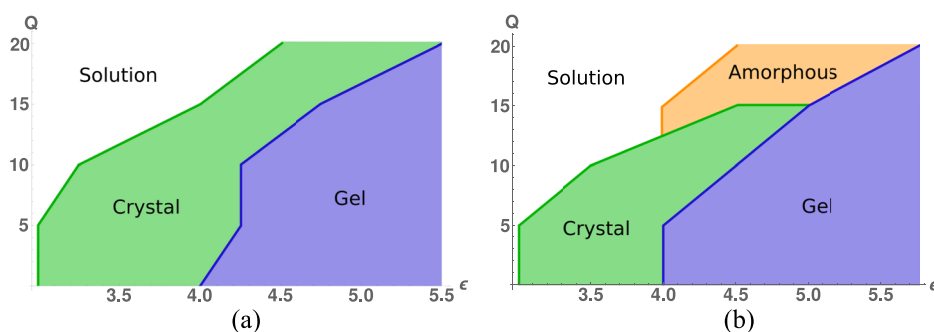

FIG. 5. Phase diagram for particles interacting by pairwise (a) and many-body (b) repulsive electrostatic potentials. The net interparticle attraction is strongest in the lower right corners where the LJ interaction parameter ϵ is large and the particle charge Q is small. Both systems show a range of interaction strengths favorable for crystal formation; however, this window is truncated in the non-pairwise system by the appearance of the amorphous state. This state exists because many-body effects lead to an enhancement of the electrostatic repulsion at high densities.
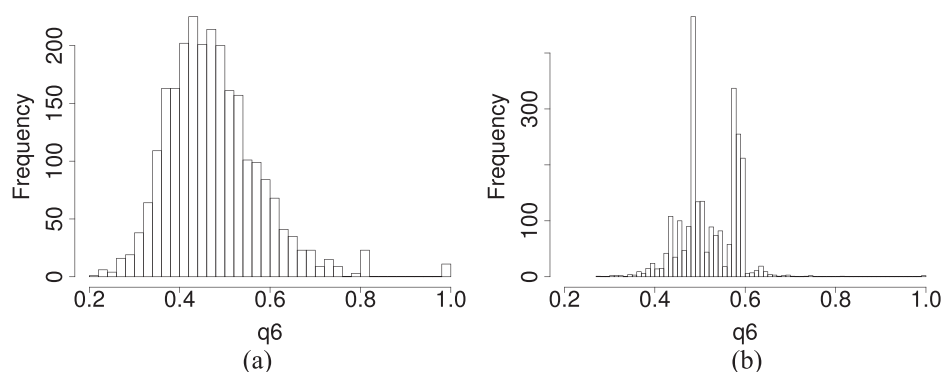
FIG. 6. Example of an amorphous structure showing no defined fcc ($q_6 = 0.57$) or hcp ($q_6 = 0.48$) indicators in local bond order (a) and a gel aggregate displaying both fcc and hcp indicator spikes (b).

and the abundance of 12-fold coordinated particles indicate that the gel has a local structure similar to the crystal. The primary difference is the much greater surface area, leading to a structure that spans the simulation box (Fig. 4). This suggests that the gel is metastable with respect to the crystal and that, with enough time, the system would minimize its surface energy by ripening into a more compact structure. The formation of a metastable state is the expected outcome at high binding energies when nucleation is fast on simulation time scales and the particle detachment events required for ripening are slow.[1,2,29]

B. Non-pairwise systems have a fourth state with an intermediate density

Figure 5 shows "phase" diagrams for systems interacting by both pairwise and non-pairwise electrostatic potentials. We stress that these states appearing in these diagrams are not necessarily true thermodynamic phases. If fact, we show (below) that the gel has crystalline order suggesting that it is a trapped state that would ripen into a crystal if given sufficient time. However, the inclusion of kinetically trapped states in the phase diagram is useful to show how electrostatic interactions should be tuned to promote the formation of ordered states.

Figure 5(a) shows the phase diagram for pairwise interacting particles. The net interaction strength is weakest in the upper left (high charge, small LJ energy) and becomes stronger moving down and to the right. This leads to the progression from liquid, to crystal, to gel as the interaction increases in strength. The phase diagram for particles interacting by a non-pairwise potential is shown in Fig. 5(b). It is similar in appearance to the phase diagram for pairwise potentials except for the appearance of a fourth state in the upper right corner. This state, which we refer to as the amorphous state, replaces the crystal phase in the highly charged region of the phase diagram.

Like the gel, the amorphous state spans the simulation box, has a high surface area, and is visually opaque (Fig. 4). Based on the coordination number criteria described above, it would be classified as a gel and, like the gel, the high surface area suggests that it could lower its free energy by ripening into a more compact structure. However, inspection of the coordination number histograms (Fig. 3) reveals that the amorphous state differs dramatically in the number of 11- and 12-fold coordinated particles, suggesting a less densely packed structure.

To further distinguish the gel and amorphous states, we employed the structural order parameter q_l [Eq. (14)], which projects the position of nearest-neighbor particles onto the spherical harmonic functions Y_{lm}.[27,28] fcc and hcp phases are readily identified by well defined peaks at $q_6 = 0.57$ and $q_6 = 0.48$, respectively. These peaks are prominent in the gel and crystal (Fig. 6). In contrast, the amorphous state lacks the defined structure in q_6, with a single broad peak spanning the range from 0.2 to 0.8.

The appearance of the amorphous state is in qualitative agreement with our prediction that the window of conditions favorable to crystallization would narrow as the strength of the short-range attraction increases.[14] This is because these systems require more electrostatic repulsion to tune the net interaction into the crystallization window, and these highly charged particles are more strongly affected by the many-body enhancement to the repulsion. For particles with sufficiently large charge, the crystal phase is no longer stable. In the simple model considered in Ref. 14, this meant that the system remained in the soluble state. Our simulations reveal that the system can also form the amorphous state as a compromise. This state allows the formation of favorable LJ interactions but retains a low enough density to prevent the many-body repulsion from overwhelming the short range attraction. The extra space required to achieve this balance prevents the system from achieving fcc, bcc, or hcp order and allows the particles to retain liquidlike disorder.

IV. CONCLUSION

Control over self-assembly requires a balance between attractive and repulsive forces. While electrostatic interactions are easily adjustable via solution conditions, the nonlinear effects of salt screening can be difficult to account for. Our simulations show that under conditions where the particles are weakly charged, a pairwise approximation can provide a good guide to system behavior. However, more highly charged systems can differ qualitatively in their behavior. These results suggest that special care needs to be taken in using dilute solution properties, such as the second virial coefficient,[30,31] to predict the formation of compact states.

ACKNOWLEDGMENTS

REFERENCES

[1] D. Rapaport, Phys. Rev. Lett. **101**, 186101 (2008).

[2] R. Jack, M. Hagan, and D. Chandler, Phys. Rev. E **76**, 021119 (2007).

[3] S. Whitelam and R. L. Jack, Annu. Rev. Phys. Chem. **66**, 143 (2015); e-print arXiv:1407.2505.

[4] A. Stradner, G. M. Thurston, and P. Schurtenberger, J. Phys.: Condens. Matter **17**, S2805 (2005).

[5] B. V. Derjaguin and L. D. Landau, Acta Physicochim. U.R.S.S. **14**, 633 (1941) [Prog. Surf. Sci. **43**, 30 (1993)].

[6] E. J. W. Verwey and J. T. G. Overbeek, *Theory of the Stability of Lyophobic Colloids* (Courier Dover Publications, 1948), p. 218.

[7] F. Sciortino, S. Mossa, E. Zaccarelli, and P. Tartaglia, Phys. Rev. Lett. **93**, 055701 (2004).

[8] S. Mossa, F. Sciortino, P. Tartaglia, and E. Zaccarelli, Langmuir **20**, 10756 (2004); e-print arXiv:0406263 [cond-mat].

[9] A. J. Archer and N. B. Wilding, Phys. Rev. E **76**, 031501 (2007).

[10] J.-M. Bomont, J.-L. Bretonnet, and D. Costa, J. Chem. Phys. **132**, 184508 (2010).

[11] L. L. Lee, M. C. Hara, S. J. Simon, F. S. Ramos, A. J. Winkle, and J.-M. Bomont, J. Chem. Phys. **132**, 074505 (2010).

[12] J. A. Bollinger and T. M. Truskett, J. Chem. Phys. **145**, 064902 (2016).

[13] Y. Zhuang and P. Charbonneau, J. Phys. Chem. B **120**, 7775 (2016).

[14] J. D. Schmit, S. Whitelam, and K. A. Dill, J. Chem. Phys. **135**, 085103 (2011).

[15] J. D. Schmit and K. A. Dill, J. Phys. Chem. B **114**, 4020 (2010).

[16] Y. R. Dahal and J. D. Schmit, Biophys. J. **114**, 76 (2018).

[17] O. Galkin and P. G. Vekilov, J. Phys. Chem. B **103**, 10965 (1999).

[18] J. C. Chen and A. S. Kim, Adv. Colloid Interface Sci. **112**, 159 (2004).

[19] J. R. Melrose, Europhys. Lett. **19**, 51 (1992).

[20] K. G. Soga, J. R. Melrose, and R. C. Ball, J. Chem. Phys. **108**, 6026 (1998).

[21] K. G. Soga, J. R. Melrose, and R. C. Ball, J. Chem. Phys. **110**, 2280 (1999).

[22] J. Theodoor and G. Overbeek, Colloids Surf. **51**, 61 (1990).

[23] K. A. Sharp and B. Honig, J. Phys. Chem. **94**, 7684 (1990).

[24] D. Andelman, *Handbook of Biological Physics* (Elsevier, 1995), Vol. 1B, pp. 603–642.

[25] J. D. Schmit, N. L. Kariyawasam, V. Needham, and P. E. Smith, J. Chem. Theory Comput. **14**, 1823 (2018).

[26] H. N. Lekkerkerker and R. Tuinier, *Colloids and the Depletion Interaction, Lecture Notes in Physics* (Springer Netherlands, Dordrecht, 2011), Vol. 833.

[27] P. J. Steinhardt, D. R. Nelson, and M. Ronchetti, Phys. Rev. B **28**, 784 (1983).

[28] W. Lechner and C. Dellago, J. Chem. Phys. **129**, 114707 (2008).

[29] S. Whitelam, E. H. Feng, M. F. Hagan, and P. L. Geissler, Soft Matter **5**, 1251 (2009).

[30] A. George and W. W. Wilson, Acta Crystallogr., Sect. D: Biol. Crystallogr. **50**, 361 (1994).

[31] A. George, Y. Chiang, B. Guo, A. Arabshahi, Z. Cai, and W. Wilson, Methods Enzymol. **276**, 100 (1997).